Multi-Layer X-ray Phase-Contrast and Dark-Field Imaging Simulator

User Manual, ver. 1.0

2024/07/17

Yongjin Sung (ysung4@uwm.edu) and Rajiv Gupta (RGUPTA1@mgh.harvard.edu)

1. Introduction

We present a simulator for X-ray phase-contrast imaging (XPCI) and X-ray dark-field imaging (XDFI). In conventional X-ray imaging, the image contrast arises from the attenuation of X-rays due to photoelectric absorption and Compton scattering. X-rays are weakly absorbed by low-atomic-number (low-Z) materials such as soft tissues. Thus, conventional X-ray imaging is unable to distinguish them despite providing excellent contrast for high-Z materials such as bones and metallic implants. Alternative approaches utilizing complementary contrast mechanisms to improve contrast in soft tissues have been explored for several decades. For example, X-ray phase-contrast imaging (XPCI) exploits X-ray refraction caused by local variations in the electron density[1]. X-ray dark-field imaging (XDFI) exploits the scramble of coherent wavefronts due to sub-structure on the micrometer scale[2]. XDFI has been shown to provide superior performance over the conventional X-ray imaging for the diagnosis of many pathologic conditions such as pulmonary fibrosis and other pulmonary diseases[3,4].

A typical X-ray simulation framework consists of two parts: a numerical phantom that provides a detailed description of human anatomy and a forward model that implements the image formation process by modeling the interaction of incident X-rays with various anatomic structures in the numerical phantom. Simulating XPCI at human scale poses challenges for both parts of the simulation framework.

For XPCI, the numerical phantom must model all the substructures responsible for phase contrast generation. In addition, voxelated numerical phantoms are unsuitable for XPCI simulation because of sharp edges and boundaries between discrete voxels. Since the X-ray phase is altered by these boundaries, the computed phase image is extensively corrupted by this artifact of how anatomy is represented and stored. XPCI also challenges the forward model for phase image computation. Ray tracing[5] or Monte Carlo[6] methods, which are commonly used by conventional X-ray simulation frameworks, cannot be used for imaging phase as they do not model phase sensitive phenomena such as coherent scattering and diffraction within the patient. These phenomena are best modelled using wave optics rather than ray tracing. Even though the use of wave optics for XPCI was demonstrated[7] as early as 1996, heretofore it has only been applied to small samples on the order of millimeters and simple geometries such as spheres and cubes.

The main challenge in human-scale XPCI/XDFI simulation is posed by the need for high computational efficiency: one must model the interaction between an X-ray wave with sub-angstrom wavelength and tissue structures that have characteristic length from hundreds of microns to tens of centimeters. Because of these modeling and computational challenges, there is no widely accepted human-scale XPCI/XDFI simulator, a technology gap that the proposed research will address by developing a publicly available, open-source simulation framework.

To overcome the limitations mentioned above, we have (1) extended the 4D cardiac-torso (XCAT) phantom—a realistic medical phantom defined with non-uniform rational B-splines (NURBS) — to enable phase contrast imaging, and (2) developed a full-wave image formation engine that uses wave optics to generate a realistic XPCI/XDFI image for an object modeled using the extended XCAT phantom[8–10]. Recently, we have further extended the full-wave simulation framework to include the dark-field signal, which arises from small-angle scattering due to unresolved, microscopic variations of refractive index in the sample[11,12]. The Multi-Layer XPCI and XDFI simulator implements our most recent algorithm in MATLAB.

Figure 1 shows the simulation geometry. The XCAT simulation provides coronal slices of a human chest. We augment the lungs by using Voronoi grids, which represent the microstructure of lungs. The wave propagation requires the complex-valued refractive index of each material that interacts with the X-ray wave. For this, we use the material IDs assigned by the XCAT and the material properties from the ICRU Report 46 “Photon, Electron, Proton and Neutron Interaction Data for Body Tissues”[13].

We first propagate a planar X-ray wave through the coronal slices to obtain the complex-valued field after the sample. The phase of the X-ray wave is modulated by the phase grating G1. The phase-modulated X-ray wave further propagates to the amplitude grating G2. The combination of G1 and G2 produces an X-ray image on the detector, which encodes the phase effects (i.e., refraction, ultra-small-angle scattering) as well as the attenuation due to the sample’s absorption. The detector records a series of images while translating the grating G2, which is to extract the attenuation, the refraction effect (called a differential phase contrast signal), and the ultra-small-angle scattering effect (called a dark-field signal) from the multiplexed intensity image. Typically, 8 images are recorded while translating the grating G2 across one full period of the grating G1.

For a more detailed description of the simulation, the users are referred to our paper.

- Y. Sung, B. Nelson, R. Gupta, “Realistic wave-optics simulation of X-ray dark-field imaging at a human scale,” arXiv:2407.12664 (2024)[14].

For a detailed description on the Talbot-Lau interferometer and the data processing, we recommend the following reference.

- M. Bech, “X-ray imaging with a grating interferometer,” Ph.D. thesis, University of Copenhagen (2009)[15].

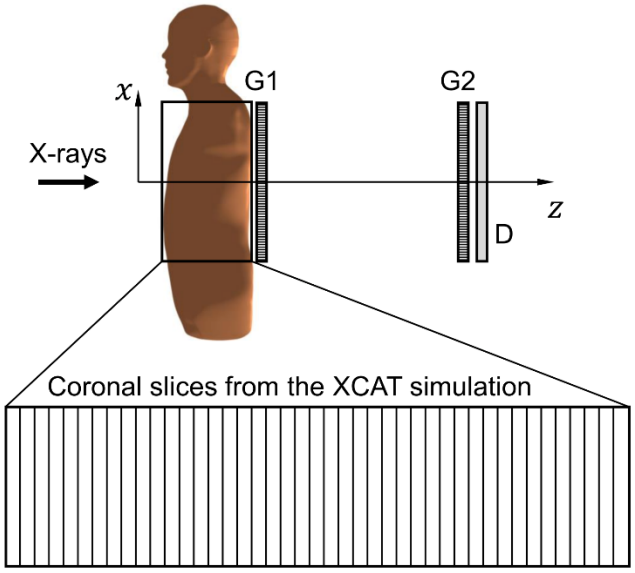

Figure 1. Schematic diagram of the simulation geometry. G1: phase grating, G2: amplitude grating, and D: detector.

2. Installation and running the program

2.1 XCAT simulation

The XCAT program can be obtained from Professor Paul Segars (paul.segars@duke.edu) at Duke University. The instructions for installing and running the XCAT are provided in the program package.

The XCAT simulation can be run on a laptop/desktop PC with a sufficient memory. To save time, we have run the XCAT simulation in a cluster using 24 CPUs, to each of which 10 GB memory is assigned. It took about five hours to generate 2505 coronal slices, each of which had 4096×4096 pixels.

The XCAT simulation needs to be performed using the file 'general.samp.par' under the main directory. Note that this file is different from the one included in the original XCAT distribution. Move the file to the directory where you installed the XCAT program. The XCAT simulation can be launched using the following command.
>> dxcat2_linux_64bit general.samp.par test

(*) The last parameter is the name that the generated image files will start with. For example, the first slice will be saved as 'test_act_1_0000.bin'.

(**) After the XCAT simulation, the generated image files should be moved to the directory 'XPCI_XDFI/raw'. Instead, the variable 'rawdir' can be changed in Part I to a user-chosen directory containing the generated image files (see Table I).

(i) Note that the default parameter setting for the XCAT will generate horizontal slices. To simulate chest X-ray imaging, we need to generate coronal slices, for which the phantom should be rotated by 90° around the x axis (according to the coordinate system defined in the XCAT program).

```
phan_rotx = 90.0        # degree to rotate the entire phantom by the x-axis
phan_roty = 0.0         # degree to rotate the entire phantom by the y-axis
phan_rotz = 0.0         # degree to rotate the entire phantom by the z-axis
```

(ii) In XCAT, the phantom can be rotated with respect to a rotation center, and the phantom can be shifted in the 3D space. After many trials, we have found the following combination places the rotated phantom near the origin of the coordinate system.

```
set_phantom_center = 1
phan_rot_centerx = 260        # rotation center (mm)
phan_rot_centery = 256
phan_rot_centerz = 1300

set_phantom_offset = 1
phan_offx = 73                # phantom offset (mm) - horizontal
phan_offy = 1195      #                       axial
phan_offz = 1022      #                       vertical
```

(iii) The following parameters determine the pixel width, the image size, the slice width, and the range of slice numbers to be used for the simulation. These numbers need to be consistent with the values used in the multi-layer simulation (Section 2.2).

```
pixel_width = 0.01    # pixel width (cm);  see NOTE 7
x_array_size = 4096   # x array size
y_array_size = 4096   # y array size

slice_width = 0.01    # slice width (cm);
startslice = 1        # start_slice;
endslice = 2505             # end_slice;
```

(iv) The slices need to be saved as separate files by turning on the 'slice_output' flag.

```
slice_output = 1
```

2.2 Multi-layer XPCI and XDFI simulation

The multi-layer XPCI and XDFI simulator is developed in MATLAB (MathWorks, Inc.). We have tested the simulator using MATLAB ver. 2021a. The simulator can be run on a laptop/desktop; however, we strongly recommend using a high-performance cluster equipped with multiple CPUs. Using a cluster with 16 CPUs, to each of which 24 GB memory was assigned, it took us about 11 days on average to complete the simulation. The majority of the computation time is currently spent to augment the lungs using Voronoi grids.

(i) A user can simply run the main program 'main.m' under the directory 'XPCI_XDFI'. The code consists of three parts. A user may change the parameters in Part I, but not those in Part II or III. The subroutines and the material database are stored in the subdirectories 'subroutines' and 'materials', respectively.

The simulated images will be saved in the subdirectory 'result'. Using the default setting, a total of 2304 files (48×48 tiles) will be generated. Each file contains the Talbot-Lau simulation result for a small tile of the chest region.

(ii) Using the code 'post.m', the raw images for different grating positions can be displayed in a montage. The subroutine 'grating_analysis' applies the Fourier analysis to the raw images and produces the attenuation ('atten'), the differential phase contrast ('dpc'), and the dark-field ('df') maps.

3. Software structure

3.1 Overview

Figure 2 shows the flowchart for the entire program, which starts with the images from the XCAT simulation (Section 2.1). In Part I, a user can set various simulation parameters that are summarized in Table I. In Part II, other parameters used for the simulation, which are summarized in Table II, are set in or calculated by the program. Note that the parameters in Part II should not be altered by a user. In Part III, the multilayer propagation is performed. Detailed steps for the Multi-Layer Propagation part are explained below. Figure 3 shows the flowcharts for Part I and Part II, and Figure 4 shows the flowchart for the Multi-Layer Propagation part.

Table I. Simulation parameters to be set by the user.

Parameters	Variable names	Default values (unit)
Energy of the X-ray source	E	50e3 (keV)
Focal spot size of the X-ray source	focalspot	1.2e-3 (m)
G0-to-G1 distance	d_g0g1	1.6 (m)
G1-to-G2 distance	d_g1g2	0.25 (m)
Lung model	lung	1

1: 'healthy'; 2: 'fibrosis'; 3: 'emphysema'; 4: emphysema (mild); 5: emphysema (moderate); 6: edema; 7: pneumonia		
Volume ratio of pus in the alveoli (used only for the pneumonia case, i.e., lung = 7)	pus_ratio	0.1
Size of the parallel pool for MATLAB parallel processing	poolsize	20
Number of layers accumulated before applying the wave propagation	skip	20
Directory for raw image files (outputs of the XCAT simulation)	rawdir	[pwd '/raw']

Table II. Other parameters set or calculated by the program

Parameters	Variable names	Value (unit)
Pixel resolution (the transverse grid size of the XCAT simulation)	res	0.01e-2 (m)
Image size (the number of pixels along each dimension)	padd0	4096
Layer thickness (the axial grid size of the XCAT simulation)	dz	0.01e-2 (m)
Division factor for subregions (the original image is divided into N×N subregions)	N	64
Margin added to each side of the subregion	marg	4
Upsampling factor	subdiv	80
Number of pixels of each subregion after adding margins and upsampling	padd1	5760
Pixel resolution after upsampling	res1	1.25 (μm)
Ratio of the detector pixel size to the image pixel size (res)	bin	4
Detector resolution	deters	400 (μm)
Number of pixels of each subregion after detector downsampling	detpxl	16
One period of the gratings (in terms of pixels)	period	8
Number of grating steps used for the data acquisition	nscan	8
Amount of phase modulation by the phase grating (G1)	dphi	π/2
One period of the grating G1	p1	10 (μm)
One period of the grating G2	p2	10 (μm)
One period of the grating G0	p0	64 (μm)

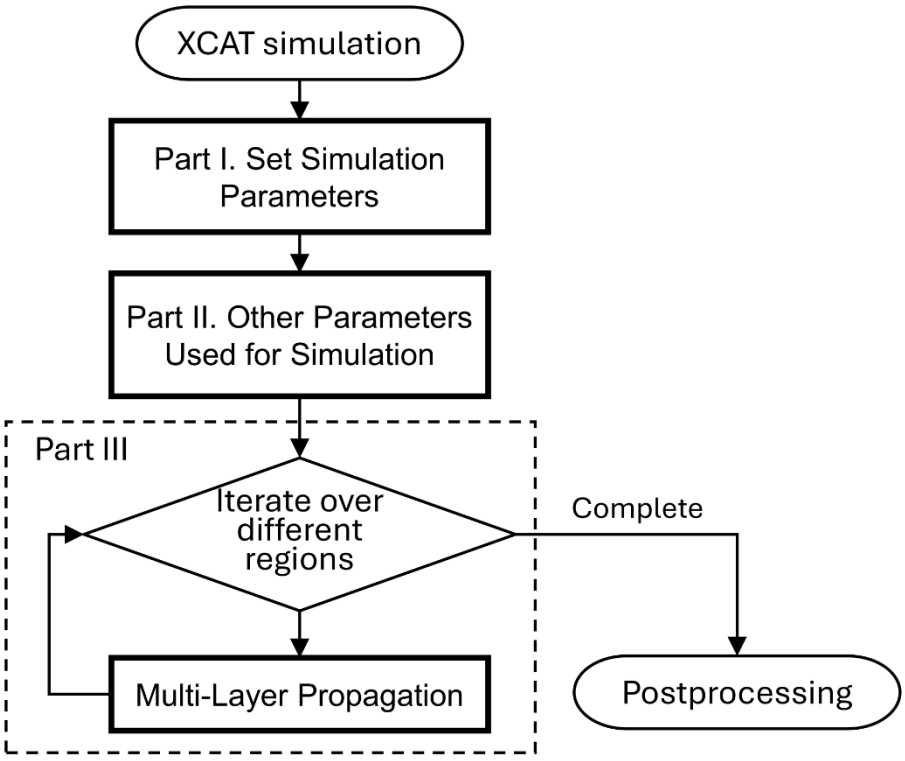

Figure 2. Flowchart for the entire program. Part I, Part II, and the Multi-Layer Propagation part are expanded in Figures 3 and 4.

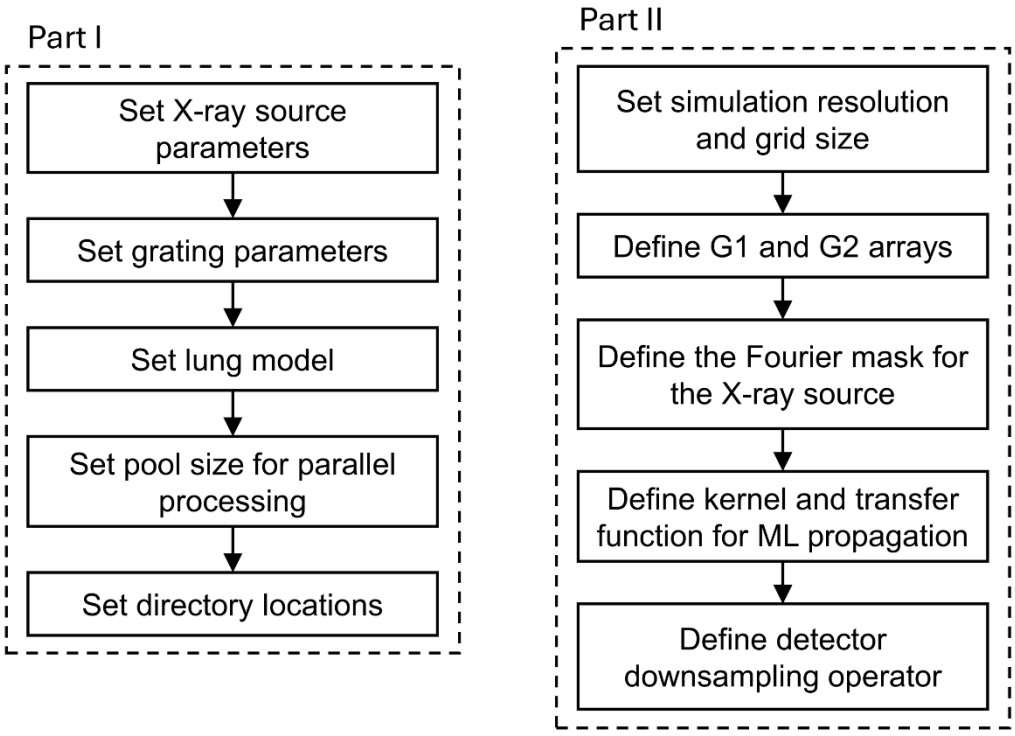

Figure 3. Flowcharts for Part I and Part II shown in Figure 2.

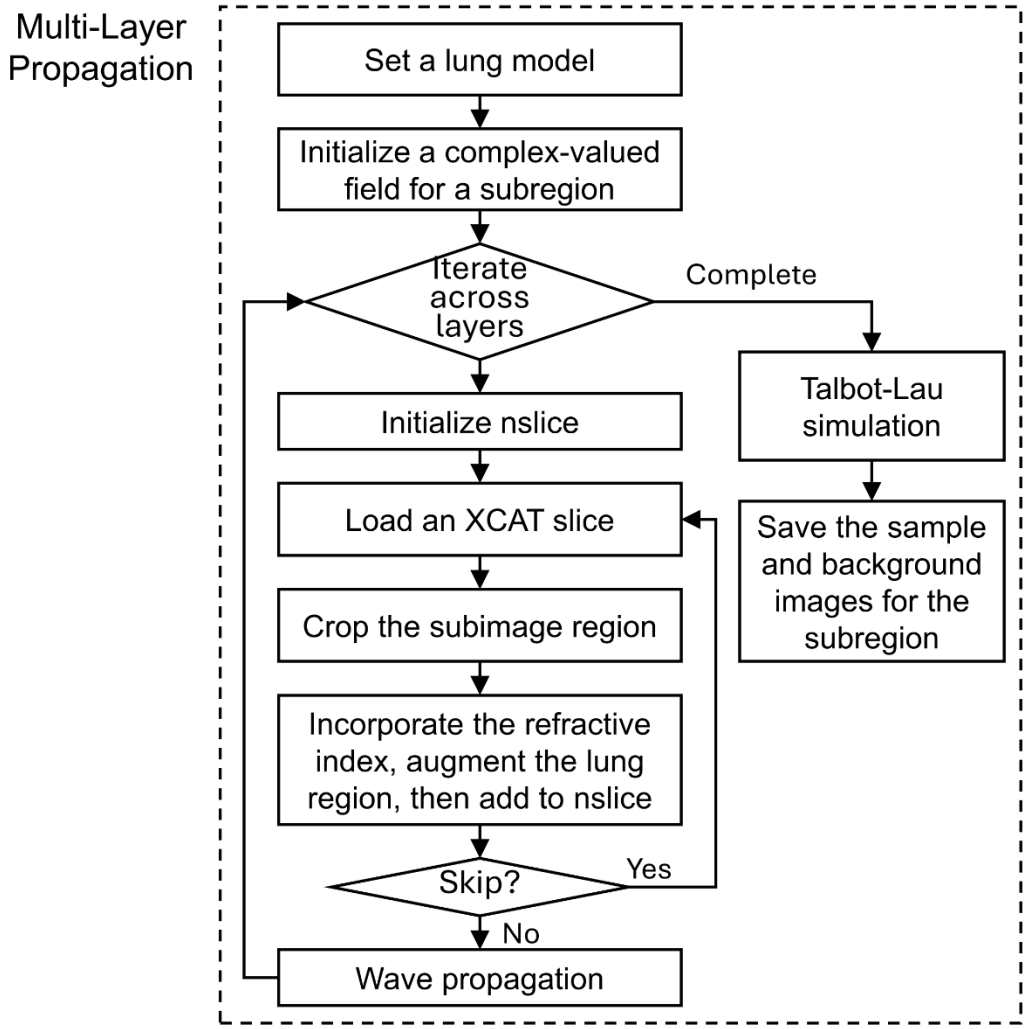

Figure 4. Flowchart for the Multi-Layer Propagation part shown in Figure 2.

3.2 Multi-Layer Propagation

The chest region is divided into N×N subregions, where N is set at 64 in Part II. The calculation for each subregion is performed independently using the parallel processing toolbox of MATLAB.

For each selected subregion, the number of alveoli ('Nalv') and the thickness of alveolus wall ('Talv') are calculated by calling the subroutine 'lung_model'. Next, a complex-valued field ('Upad') is initialized as a 2D array of one with the size padd1×padd1, where 'padd1' is set as 5760 in Part II. Then, the XCAT images will be sequentially loaded to calculate 'Upad' after the sample (i.e., at the plane where the grating G1 is placed). 'Upad' is updated as follows.

First, an XCAT image (i.e., a coronal slice from the XCAT simulation) in the sequence is loaded by calling the subroutine 'load_image'. A subregion is selected by calling the subroutine 'select_subimage'. The values in the image are the organ IDs obtained from the XCAT simulation. The complex refractive index value for each organ ID can be obtained from the ICRU Report 46 database.

The subroutine 'get_nslice' assigns the complex refractive index value to each organ in the selected subregion of the XCAT image. It also upsamples the image by a factor of 'subdiv', which is set as 80 in Part II. Figure 5 shows the grids used at different steps of the simulation, and Table III summarizes the number of pixels and the pixel size of each grid. If there are lungs, the slice is upsampled then the lung region is augmented using the Voronoi grids, as described in Section 3.3. The subroutine 'get_nslice' can be used for all the lung models except for pneumonia. For the pneumonia case, the subroutine 'get_nslice_pneumonia' is used instead.

Table III. Grids used at different steps of the simulation.

Simulation step	1	2	3	4	5	6
Number of pixels along each dimension	padd0 = 4096	padd0 /N = 64	padd0/N + 2×margin = 72	padd1 = (padd0/N+2×margin)×subdiv = 5760	padd0/N/bin + 2×margin/bin = 18	padd0/ N/bin = 16
Pixel size	res = 100 μm			res1 = res/subdiv = 1.25 μm	res×bin = 400 μm	

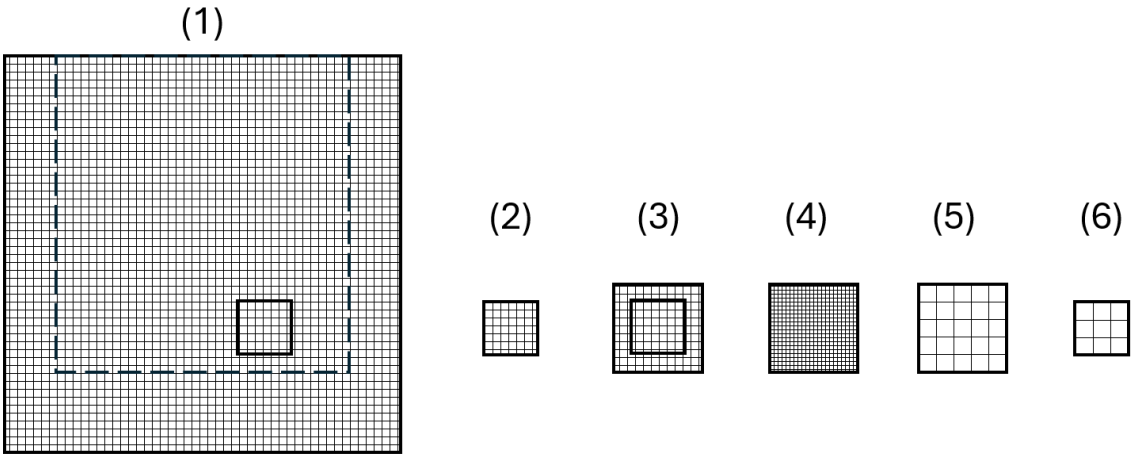

Figure 5. Grids used at different steps of the simulation: (1) at the beginning (the original image from the XCAT); (2) after the selection of a subregion (1/N along each dimension); (3) after adding a margin (marg) to each side of the selected subregion; (4) after upsampling the padded subregion by a factor of subdiv, to which the wave propagation is applied; (5) after the integration downsampling by the detector; and (6) after removing the margin. Table III

summarizes the number of pixels along each dimension and the pixel size (i.e., grid spacing). The dashed line in (1) marks the region used for XPCI/XDFI simulation.

The output of the subroutine ‘get_nslice’ is temporarily saved in the variable ‘tmp’. When axial averaging is not used, ‘tmp’ will be simply reassigned to the variable ‘nslice’. The axial averaging may be used to reduce the computation time by performing the wave propagation every ‘skip’ images, where skip can be set in Part I (default value: 20). With the axial averaging, ‘nslice’ stores the average of the slices (i.e., the outputs of ‘get_nslice’) and calls the subroutine ‘ML_prop_dz’ after every ‘skip’ images. After that, ‘nslice’ is initialized to zero and continues to accumulate the slices until the next wave propagation. The kernel ‘Prop’ required for the multi-layer propagation is calculated by the subroutine ‘ML_kernel’ in Part II. The same kernel is used for every slice.

When the wave propagation reaches the last slice in the sequence, the Talbot-Lau simulation is performed by calling the subroutine ‘grating_stepping’. The subroutine produces the sample (‘Is’) and background (‘Ibg’) images for ‘nscan’ grating positions, where ‘nscan’ is set as 8 in Part II, as described in Section 3.4. Last, ‘Is’ and ‘Ibg’ are saved as a mat file.

3.3 Assignment of complex refractive index and augmentation of the lung model using Voronoi grids

The augmentation is applied only to the lung regions. For the slices not including lungs, the augmentation is skipped. In the subroutine ‘get_nslice’, the IDs of the organs included in the selected subregion are first obtained. For the identified organ IDs, the complex refractive index value is obtained for the X-ray energy ‘E’ by calling the subroutine ‘organ_refr_ind’. To each organ ID, a material composition is assigned—the information stored in the file ‘materials\id_to_mater_comp.mat’. Note that an organ may be made of multiple materials. The file ‘id_to_mater_comp.mat’ stores the material IDs and their concentrations for each organ ID in two containers.Map ‘M1’ and ‘M2’, respectively. The complex refractive index for a composite material is calculated as a weighted sum of the refractive indices for the constituents. The obtained refractive index is assigned to each organ in the slice. Table IV summarizes the material IDs assigned in the XCAT.

If lungs are not included in the selected subregion, the slice is simply upsampled by a factor of ‘subdiv’, which is set as 80 in Part II. If lungs are included, Voronoi grids are generated. The complex refractive index for the lung material (material ID: 2) is assigned to the alveolus walls (i.e., Voronoi boundaries). To the inner region of each Voronoi cell, the complex refractive index for air (material ID: 22) is assigned.

Table IV. Material ID defined in XCAT and example complex refractive index for the X-ray energy of 50 keV. The complex refractive index is given as $1 - \delta + i\beta$.

Material ID	Materials	Complex refractive index	
		δ ($\times 10^{-7}$)	β ($\times 10^{-10}$)
0	Water	0.921	0.448
1	Muscle	0.960	0.468
2	Lung	0.951	0.466
3	Dry spine	1.249	0.953
4	Dry rib	1.241	0.940
5	Adipose	0.877	0.397
6	Blood	0.968	0.477
7	Heart	0.968	0.477
8	Kidney	0.960	0.468
9	Liver	0.968	0.475
10	Lymph	0.943	0.463
11	Pancreas	0.954	0.462
12	Intestine	0.943	0.457
13	Skull	1.398	1.204
14	Cartilage	0.998	0.506
15	Brain	0.954	0.466
16	Spleen	0.968	0.475
22	Air	0.000999	0.0004946
26	Skin	0.993	0.480
30	Red marrow	0.943	0.447
31	Yellow marrow	0.905	0.408
32	Testis	0.954	0.466
33	Thyroid	0.960	0.491
34	Bladder	0.946	0.467

3.4 Talbot-Lau simulation

The subroutine ‘grating_stepping’ takes the complex-valued field after the sample (‘Upad’) as an input and generates the sample (‘Is’) and background (‘Ibg’) images that a Talbot-Lau interferometer would produce. For ‘nscan’ grating positions, where ‘nscan’ is set as 8 in Part II, the sample images ‘Is’ are generated. The background images are the images recorded without the sample for the same grating positions.

For each grating position, ‘Upad’ is multiplied with a phase mask for the grating G1 (‘g1’). The phase mask has a period of ‘p1’, which is set at 10 μm in Part II, producing a phase modulation of ‘dphi’, which is set at π/2 in Part II. Note that the amplitude distribution is not altered by the phase mask. After being multiplied with the phase mask, the complex-valued field is propagated to the

G2 plane, where the amplitude grating G2 is placed, then is multiplied with the amplitude mask ‘bimask2’. The amplitude mask has the period of ‘p2’, which is set as 10 μm in Part II.

The detector is located right after the grating G2. Note that the detector records the intensity of X-rays, not their complex-valued field. The intensity of X-rays after the grating G2 is convoluted with a 2D smoothing function, which accounts for a finite focal spot size of the X-ray source (also known as penumbral blur). The 2D smoothing function is calculated in Part II by the subroutine ‘define_source’. As the detector pixel is much larger than the simulation resolution, the intensity needs to be downsampled. The integration downsampling is represented by the matrix ‘DS’, which is calculated by the subroutine ‘downsamp’ in Part II.

The sample and background intensity images for ‘nscan’ grating positions are saved as ‘Is’ and ‘Ibg’, respectively, and returned.

Acknowledgment

This work was supported by the National Institutes of Health (NIBIB) under Grant 1R03EB032038.

References

1. Paganin D. Coherent X-ray Optics. Oxford University Press; 2006.

2. Pfeiffer F, Bech M, Bunk O, Kraft P, Eikenberry EF, Brönnimann C, Grünzweig C, David C. Hard-X-ray dark-field imaging using a grating interferometer. Nat Mater. Nature Publishing Group; 2008;7(2):134–137.

3. Gassert FT, Urban T, Frank M, Willer K, Noichl W, Buchberger P, Schick R, Koehler T, von Berg J, Fingerle AA. X-ray dark-field chest imaging: qualitative and quantitative results in healthy humans. Radiology. Radiological Society of North America; 2021;301(2):389–395.

4. Willer K, Fingerle AA, Gromann LB, De Marco F, Herzen J, Achterhold K, Gleich B, Muenzel D, Scherer K, Renz M. X-ray dark-field imaging of the human lung—A feasibility study on a deceased body. PLoS One. Public Library of Science San Francisco, CA USA; 2018;13(9):e0204565.

5. Fung YC. A model of the lung structure and its validation. J Appl Physiol. 1988;64(5):2132–2141.

6. Jones DG, Wall BF. Organ doses from medical x-ray examinations calculated using Monte Carlo techniques. National Radiological Protection Board; 1985.

7. Wilkins SW, Gureyev TE, Gao D, Pogany A, Stevenson AW. Phase-contrast imaging using polychromatic hard X-rays. Nature. Nature Publishing Group; 1996;384(6607):335–338.

8. Sung Y, Sheppard CJ, Barbastathis G, Ando M, Gupta R. Full-wave approach for x-ray phase imaging. Opt Express. Optica Publishing Group; 2013;21(15):17547–17557.

9. Sung Y, Segars WP, Pan A, Ando M, Sheppard CJ, Gupta R. Realistic wave-optics simulation of X-ray phase-contrast imaging at a human scale. Sci Rep. Nature Publishing Group; 2015;5(1):1–10.

10. Sung Y, Nelson B, Shanblatt ER, Gupta R, McCollough CH, Graves WS. Wave optics simulation of grating-based X-ray phase-contrast imaging using 4D Mouse Whole Body (MOBY) phantom. Med Phys. Wiley Online Library; 2020;47(11):5761–5771.

11. Yashiro W, Terui Y, Kawabata K, Momose A. On the origin of visibility contrast in x-ray Talbot interferometry. Opt Express. 2010;18(16):16890–16901.

12. Lynch SK, Pai V, Auxier J, Stein AF, Bennett EE, Kemble CK, Xiao X, Lee WK, Morgan NY, Wen HH. Interpretation of dark-field contrast and particle-size selectivity in grating interferometers. Appl Opt. Optical Society of America; 2011;50(22):4310–4319.

13. White DR, Griffith RV, Wilson IJ. Photon, electron, proton and neutron interaction data for body tissues. ICRU Rep 46. 1992;46.

14. Sung Y, Nelson B, Gupta R. Realistic wave-optics simulation of X-ray dark-field imaging at a human scale [Internet]. arXiv; 2024 [cited 2024 Jul 17]. Available from: http://arxiv.org/abs/2407.12664

15. Bech M, Tapfer A, Velroyen A, Yaroshenko A, Pauwels B, Hostens J, Bruyndonckx P, Sasov A, Pfeiffer F. In-vivo dark-field and phase-contrast x-ray imaging. Sci Rep. Nature Publishing Group; 2013;3(1):1–3.